Low-Temperature Kinetics of Reactions of OH Radical with Ethene, Propene, and 1-Butene

Andrei B. Vakhtin,[†] James E. Murphy,[‡] and Stephen R. Leone*[,§]

JILA, National Institute of Standards and Technology and University of Colorado, and Department of Chemistry and Biochemistry, University of Colorado, Boulder, Colorado 80309-0440

Received: February 20, 2003; In Final Form: June 30, 2003

The kinetics of the reactions of the OH radical with ethene (k_1), propene (k_2), and 1-butene (k_3) are studied over a temperature range of $T = 96-296$ K. The low-temperature environment is provided by a pulsed Laval nozzle supersonic expansion of nitrogen with admixed radical precursor and reactant gases. The OH radicals are produced by pulsed photolysis of H_2O_2 at 248 nm. Laser-induced fluorescence of the OH radicals excited in the (1,0) band of the $A^2\Sigma^+-X^2\Pi_i$ transition is used to monitor the OH decay kinetics to obtain the bimolecular rate coefficients. At $T = 296$ K, the rate constants k_1, k_2, and k_3 are also measured as a function of total pressure. The room-temperature falloff parameters are used as the basis for extrapolation of the low-temperature kinetic data, obtained over a limited range of gas number density, to predict the high-pressure limits of all three rate coefficients at low temperatures. The temperature dependence of the measured high-pressure rate constants for $T = 96-296$ K can be expressed as follows: $k_{1,\infty} = (8.7 \pm 0.7) \times 10^{-12}(T/300)^{(-0.85\pm0.11)}$ cm^3 molecule^{-1} s^{-1}; $k_{2,\infty} = (2.95 \pm 0.10) \times 10^{-11}(T/300)^{(-1.06\pm0.13)}$ cm^3 molecule^{-1} s^{-1}; $k_{3,\infty} = (3.02 \pm 0.15) \times 10^{-11}(T/300)^{(-1.44\pm0.10)}$ cm^3 molecule^{-1} s^{-1}. All three high-pressure rate constants show a slight negative temperature dependence, which is generally in agreement with both low-temperature and high-temperature kinetic data available in the literature. Implications to the atmospheric chemistry of Saturn are discussed. Incorporating the new experimental data on k_1 in photochemical models of Saturn's atmosphere may significantly increase the predicted rate of photochemical conversion of H_2O into C−O containing molecules.

Introduction

In a previous paper we reported measurements of the rate constants of the reactions of hydroxyl radical OH with propene and 1-butene at $T = 103$ and 298 K using a pulsed Laval nozzle apparatus.[1] Both measured rate constants agreed well with available low-temperature and high-temperature kinetic data, showing a slight negative temperature dependence. At low and moderate temperatures, reactions of OH with alkenes proceed by addition;[2−9] therefore, in general, the corresponding rate constants should be pressure-dependent. In the initial study[1] we assumed that the rate constants for the OH + propene and OH + 1-butene reactions measured at $T = 103$ K and a total gas number density of about 2×10^{16} molecule cm^{-3} are at, or very close to, the high-pressure limit. This assumption is reasonable in view of the considerable complexity of the species involved in the reactions. Moreover, comparison of the rate constants measured at room temperature and similar total gas densities with literature data shows that the 2×10^{16} molecule cm^{-3} gas number density provides essentially high-pressure conditions for these two reactions even at room temperature. However, our estimates indicate that the high-pressure limit would not be the case for the reaction of OH with ethene. For this reaction, analysis of the pressure dependence of the rate constant is required even at temperatures as low as 100 K. In this paper we report new kinetic data on the reactions of OH with ethene, propene, and 1-butene:

$$OH + C_2H_4 (+ M) \xrightarrow{k_1} C_2H_4OH (+ M) \qquad (R1)$$

$$OH + C_3H_6 (+ M) \xrightarrow{k_2} C_3H_6OH (+ M) \qquad (R2)$$

$$OH + C_4H_8 (+ M) \xrightarrow{k_3} C_4H_8OH (+ M) \qquad (R3)$$

obtained over a temperature range of $T = 96-296$ K. As indicated by the reaction equations, we assume that all three reactions proceed by addition at low temperatures. The rate constants k_1, k_2, and k_3 are measured as a function of total pressure at $T = 296$ K, and the room-temperature falloff parameters are used to extrapolate the low-temperature data for k_1, k_2, and k_3 (obtained for a limited range of total gas number densities) to the high-pressure limit. The obtained rate constants are compared to the available literature data and are also discussed in terms of possible applications to the photochemical models of the atmospheres of the outer planets.

Experimental Section

The apparatus used in this work has been described previously.[1,10] Therefore, only a brief description will be given here. The low-temperature environment is created by supersonic expansion of gas through a Laval nozzle. The Laval nozzle block is mounted inside a stainless steel chamber. The nozzle block can be translated about 30 cm along the chamber axis. Two homemade pulsed valves driven by piezo disk translators supply a gas pulse of approximately 5-ms duration (nitrogen with

* Corresponding author.
[†] Present address: Southwest Sciences, Inc., Santa Fe, NM 87544. E-mail: avakhtin@swsciences.com.
[‡] Present address: National Renewable Energy Laboratory, Golden, CO 80401. E-mail: murphyje@mail.colorado.edu.
[§] Present Address: Departments of Chemistry and Physics, and Lawrence Berkeley National Laboratory, University of California, Berkeley, CA 94720. E-mail: srl@cchem.berkeley.edu.

10.1021/jp030230a CCC: $25.00
Published on Web 11/04/2003

TABLE 1: Characterization of the Three Laval Nozzles, Used in the Kinetic Experiments, by Different Methods

	Pitot tube measurements				OH LIF excitation spectra	direct measurements of the flow velocity
nozzle	Mach number	gas number density, molecules cm^{-3}	temp, K	flow velocity, cm/s	temp, K	flow velocity, cm/ s
1	2.01 ± 0.19	$(3.5 \pm 0.7) \times 10^{16}$	165 ± 14	$(5.34 \pm 0.30) \times 10^4$	152 ± 14	$(5.34 \pm 0.10) \times 10^4$
2	2.93 ± 0.14	$(2.65 \pm 0.45) \times 10^{16}$	110 ± 7	$(6.24 \pm 0.12) \times 10^4$	109 ± 16	$(6.21 \pm 0.12) \times 10^4$
3	3.24 ± 0.10	$(1.9 \pm 0.2) \times 10^{16}$	96 ± 4	$(6.48 \pm 0.07) \times 10^4$	94 ± 8	$(6.47 \pm 0.09) \times 10^4$

admixed radical precursor and reactant gases) to the preexpansion chamber of the nozzle block. The gas expands through the Laval nozzle to the chamber pumped by a mechanical pump (60 L/s). The expansion results in a collimated supersonic gas flow, which is characterized by uniform Mach number, gas number density, and temperature along the flow axis for about 20 cm.[1,10] The variable opening of a gate valve is used to control the pumping speed in order to optimize the background pressure for the appropriate collimation of the supersonic flow. The background pressure in the chamber is measured by a capacitance manometer. With three different Laval nozzles used in the present work, the kinetic measurements can be performed in a temperature range of 96−165 K. The Mach number, temperature, gas number density, and static pressure in the supersonic flow are characterized by Pitot tube measurements,[11] as described earlier.[1,10] The static pressure of the flow obtained from the Pitot tube measurements is in reasonably good agreement with the background pressure in the chamber adjusted to obtain a collimated supersonic flow. For the three nozzles used in the experiments, the difference was not more than 13%. The temperature in the flow can also be tested independently by analysis of the rotational structure of laser-induced fluorescence (LIF) excitation spectra of the OH radical.[1] In this paper, we use an additional means of flow diagnostics, namely, direct measurement of its velocity, based on measurements of the OH radical LIF signal versus distance between the nozzle and photomultiplier (see Results).

The chamber and the nozzle block have quartz windows, which makes it possible to introduce laser beams along the axis of the gas flow to generate radicals photolytically (an excimer laser) and for laser-based diagnostics (tunable frequency-doubled dye laser). In this work, LIF from OH is used as a probe. The output flange of the chamber is equipped with a baffle arm ending in a quartz Brewster angle window to minimize the scattered light.

The OH radicals are produced by pulsed photolysis of H_2O_2 at 248 nm with the unfocused beam of a KrF excimer laser (up to 100 mJ/pulse at a repetition rate of 10 Hz). The frequency-doubled output radiation of a pulsed dye laser operating on Rhodamine 590 dye and pumped by the second harmonic of a Nd:YAG laser is used for excitation of LIF in the $Q_1(1)$ line of the (1,0) band of the $A^2\Sigma^+ - X^2\Pi_i$ transition of OH. LIF from OH is detected on the (1,1) and (0,0) bands of the A−X transition by a photomultiplier tube (PMT) equipped with a UG-11 UV band-pass filter and a narrow-band interference filter (310 ± 10 nm). The PMT, mounted 15 cm downstream of the nozzle, detects the light that is collected by a quartz lens (5 cm in diameter and 5-cm focal length). The lens focuses the image of a segment of the irradiated zone, which is about 2 cm long, to the PMT photocathode. The optics are appropriately shielded to minimize the effect of scattered light.

The kinetics of the OH decay are traced by monitoring the OH LIF intensity versus delay between the photolysis and probe laser pulses. Typically, the signal from the photomultiplier is integrated over a 200-ns gate after a delay of 200 ns with respect to the excitation laser pulse by a boxcar averager. Active background subtraction is performed by setting the photolysis−probe delay to a negative value for every other triggering pulse and subtracting the background from the signal. Normally, each OH decay profile is obtained as an average of 20−100 experimental kinetic curves. Each kinetic curve consists of 20 points (signal minus background) covering a probe delay time interval of 10−200 μs in 10-μs steps and takes 4 s to be acquired (at 10-Hz pulse repetition rate). The triggering of all units and devices is provided by a four-channel digital delay/pulse generator. Both the boxcar integrator and the pulse generator are GPIB-interfaced to a PC computer, which is used to control the experiment and for data acquisition.

The gas flows, supplied from cylinders through stainless steel lines and controlled by mass flow controllers, are mixed in a 150-cm^3 stainless steel cylinder on their way to the nozzle block. A controlled flow of N_2 is bubbled through a sample of a concentrated (>90%) aqueous solution of hydrogen peroxide and then mixed into the main flow of the carrier gas. The total gas number density in the collimated supersonic flow is measured by the Pitot tube method,[11] as described in the earlier work.[1] The gas number densities for individual components are calculated from the total density and the known relative mass flows. The flow controllers are calibrated for individual gases by measuring the rate of filling a known volume to a known pressure.

The gases used are as follows: N_2 (99.999%); ethene (99.999%); propene (99.97%); 1-butene (99.9%). All gases are used as supplied without purification.

Results and Discussion

Characterization of the Supersonic Flow: Direct Measurement of Flow Velocity. In this work, three Laval nozzles are used to provide different low-temperature environments at different temperatures. The supersonic flows produced by the nozzles are characterized by Pitot tube measurements and LIF spectroscopy of OH radicals. The characterization procedures have been described in detail elsewhere.[1] The results of these measurements for the three nozzles are summarized in Table 1. As seen from Table 1, uncertainties in temperature and gas number density are relatively high (especially for nozzle no. 1). These uncertainties are caused mainly by inhomogeneity of the collimated supersonic flow and are treated as systematic errors in evaluating the final uncertainties reported for the measured rate constants.[1]

We also use a direct method of determination of the flow velocity, which provides complementary information. To measure the flow velocity we take advantage of a spike in the OH concentration time profile that is produced by the photolysis of H_2O_2 in the preexpansion chamber of the Laval nozzle block (see Figure 1a). The preexpansion chamber is relatively small, and most of its volume is irradiated by the photolysis laser beam. When the portion of the gas irradiated in the preexpansion chamber expands through the nozzle, the OH radicals fill the whole aperture of the flow (in contrast to the OH produced in the supersonic flow, where OH radicals are formed only within the laser beam aperture diameter). Since the gas flow diameter

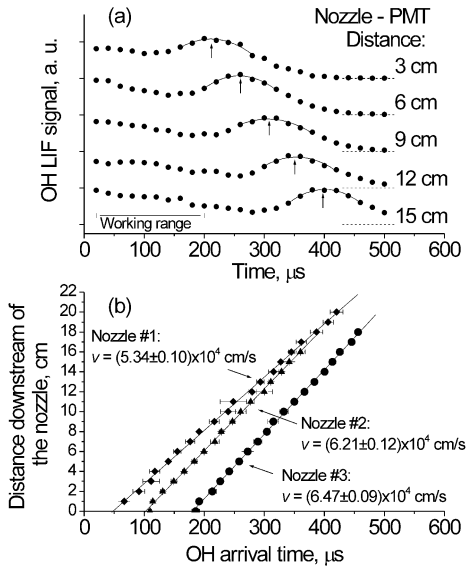

Figure 1. (a) Points show the OH time profiles obtained in the photolysis of H_2O_2 in supersonic expansion through Laval nozzle no. 3 (Mach number 3.24) at different nozzle−PMT distances. For each data set, lines represent the parabolic fits to the seven points closest to the maximum of the spike. Arrows show the positions of the maxima of the spikes in OH time profiles that correspond to OH produced in the preexpansion chamber (see text). The time window for kinetic studies (which are performed at a nozzle−PMT distance of 15 cm) is indicated as the "working range". (b) The arrival times of the spikes in OH time profiles plotted in time−distance coordinates for the three nozzles used in this study. The flow velocities obtained from the slopes are indicated.

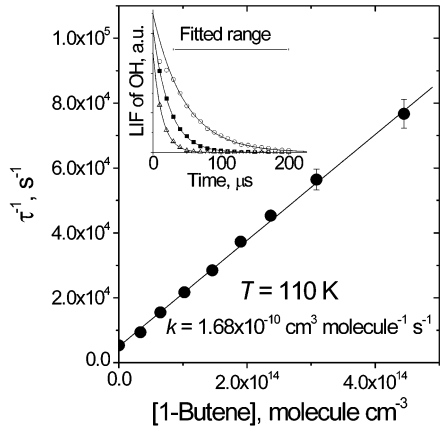

Figure 2. Reciprocal OH decay time versus reactant concentration for the OH + C_4H_8 reaction obtained at $T = 110$ K. For each concentration, the error bars indicate two standard deviations of the fit of the experimental kinetic curves by a single-exponential function. The line shows the $1/\sigma^2$-weighted linear fit. The inset shows representative examples of the OH decay profiles obtained at different 1-butene concentrations: 1.0×10^{14} molecule cm^{-3} (open circles); 2.4×10^{14} molecule cm^{-3} (filled squares); 4.4×10^{14} molecule cm^{-3} (open triangles).

is 2−4 times larger than the laser beam diameter, the radial diffusion of the radicals from the center of the flow (where the OH radicals are detected by LIF) is different (slower) for the portion of the flow where the radicals are formed before the expansion. This leads to the appearance of a spike in the OH radical profile. Another reason for the OH spike formation could be a difference in the absorption cross-section of H_2O_2 at 248 nm at low temperatures (in the supersonic flow) and at room temperature (in the preexpansion region).[12,13] Note that only the uniform part of the OH profile (with nozzle−PMT distance equal to 15 cm) is used for kinetic studies (marked as the "working range" in Figure 1a). The portion of the OH profile with the spike is used only for the flow velocity measurements.

To measure the flow velocity, the OH time profiles are recorded at different distances between the Laval nozzle and the PMT (see Figure 1a). The arrival time of the maximum of the spike is determined for each nozzle−PMT distance by fitting the seven points closest to the maximum of the spike by a second-order polynomial for each data set (lines in Figure 1a). Then the data are plotted in distance−time coordinates. Figure 1b shows the results obtained for the three nozzles. The slopes of the linear fits of the experimental data give the flow velocities directly. The results of the direct velocity measurements are presented in Table 1 and are seen to be in excellent agreement with both the Pitot tube data and the OH rotational temperatures obtained by LIF. In this work we use a simplified procedure to estimate the OH rotational temperature that involves consideration of relative intensities of the rotational lines belonging to only two branches, R_1 and Q_{21}, of the LIF excitation spectra of the OH radical in the (1,0) band of the $A^2\Sigma^+-X^2\Pi$ transition (obtained at the photolysis−probe delay of 30 μs). This procedure produces higher uncertainty, compared with the Pitot tube measurements. The supersonic flow parameters derived from Pitot tube measurements are considered the most reliable. The direct OH LIF flow velocity measurements have smaller uncertainty for the no. 1 nozzle but give excellent agreement with the Pitot tube measurements. The Pitot measurements are used to characterize the experimental conditions for the kinetic studies described in the following sections.

Rate Constants for the Reactions of OH with Ethene, Propene, and 1-Butene. The low-temperature rate constants of the reactions R1, R2, and R3 are measured using the pulsed Laval nozzle expansion method and LIF detection of the disappearance of the OH radicals. The inset in Figure 2 shows representative examples of OH decay profiles obtained at different concentrations of 1-butene at $T = 110$ K. Similar results have been obtained for OH decay kinetics in the presence of ethene and propene. In all cases, the kinetic curves are well described by a single-exponential decay function. To ensure that the OH rotational relaxation effects[14,15] do not interfere with the OH reactive decay kinetics, we neglect the first two points of the experimental kinetic curves in the fitting procedure; i.e., we fit only the tails of the OH time profiles, starting at a 30-μs photolysis−probe delay (the fitted data range is shown by the horizontal arrow in the inset in Figure 2). To obtain the rate constants, the OH decay time is measured as a function of alkene concentration, which is varied over at least a factor of 10. A representative example of the pseudo-first-order plot for reaction R3 is shown in Figure 2. The corresponding rate constant can be obtained from the slope of the straight line that fits the experimental dependence. The intercept is primarily due to the diffusion loss of the OH radicals out of the detection zone. We estimate the OH concentration immediately after the photolysis pulse to be $< 3 \times 10^{10}$ molecule cm^{-3}, which is about 3 orders of magnitude less than the smallest alkene concentration used in kinetic measurements. Therefore, self-reaction of OH can probably be neglected. However, a certain contribution of the reaction of OH with H_2O_2 cannot be excluded. The rate constant for this reaction at room temperature is 1.7×10^{-12} cm^3 molecule^{-1} s^{-1},[16] and low-temperature measurements of this rate constant are underway in this laboratory. The rate constants for reactions R1, R2, and R3 measured at different temperatures and gas number densities, as well as the details of the experimental conditions, are presented in Tables 2−4. The

TABLE 2: Rate Constants for the OH + C_2H_4 Reaction (k_1). Buffer Gas N_2

T, K	total gas density, molecule cm^{-3}	$[C_2H_4]$, molecule cm^{-3}	rate constant,[a] cm^3 molecule^{-1} s^{-1}
96 ± 4	$(1.9 \pm 0.2) \times 10^{16}$	$(0-6.3) \times 10^{14}$	$(1.99 \pm 0.33) \times 10^{-11}$
110 ± 7	$(2.65 \pm 0.45) \times 10^{16}$	$(0-7.2) \times 10^{14}$	$(1.74 \pm 0.40) \times 10^{-11}$
165 ± 14	$(3.5 \pm 0.7) \times 10^{16}$	$(0-1.6) \times 10^{15}$	$(7.20 \pm 1.80) \times 10^{-12}$
296 ± 2	2.85×10^{16}	$(0-1.6) \times 10^{15}$	$(1.54 \pm 0.19) \times 10^{-12}$
296 ± 2	4.74×10^{16}	$(0-2.6) \times 10^{15}$	$(2.03 \pm 0.21) \times 10^{-12}$
296 ± 2	8.06×10^{16}	$(0-4.3) \times 10^{15}$	$(2.72 \pm 0.30) \times 10^{-12}$
296 ± 2	1.07×10^{17}	$(0-5.8) \times 10^{15}$	$(3.04 \pm 0.33) \times 10^{-12}$
296 ± 2	1.68×10^{17}	$(0-9.6) \times 10^{15}$	$(3.60 \pm 0.46) \times 10^{-12}$
296 ± 2	2.34×10^{17}	$(0-6.5) \times 10^{15}$	$(4.43 \pm 0.54) \times 10^{-12}$
296 ± 2	3.27×10^{17}	$(0-6.6) \times 10^{15}$	$(5.09 \pm 0.59) \times 10^{-12}$
296 ± 2	4.85×10^{17}	$(0-5.1) \times 10^{15}$	$(5.02 \pm 0.62) \times 10^{-12}$
296 ± 2	7.11×10^{17}	$(0-4.2) \times 10^{15}$	$(5.48 \pm 0.58) \times 10^{-12}$
296 ± 2	9.72×10^{17}	$(0-3.5) \times 10^{15}$	$(5.59 \pm 0.59) \times 10^{-12}$
296 ± 2	1.65×10^{18}	$(0-6.6) \times 10^{15}$	$(6.17 \pm 0.67) \times 10^{-12}$
296 ± 2	3.25×10^{18}	$(0-7.1) \times 10^{15}$	$(6.80 \pm 0.76) \times 10^{-12}$

[a] The indicated uncertainties are represented as $\pm 2\sigma_c$, where σ_c is a "combined standard uncertainty" that accumulates both statistical and systematic errors (see text).

TABLE 3: Rate Constants for the OH + C_3H_6 Reaction (k_2). Buffer Gas N_2

T, K	total gas density, molecule cm^{-3}	$[C_3H_6]$, molecule cm^{-3}	rate constant,[a] cm^3 molecule^{-1} s^{-1}
96 ± 4	$(1.9 \pm 0.2) \times 10^{16}$	$(0-4.6) \times 10^{14}$	$(1.29 \pm 0.29) \times 10^{-10}$
103 ± 9	2.1×10^{16}	$(0-3.8) \times 10^{14}$	$(8.1 \pm 1.8) \times 10^{-11}$ [b]
165 ± 14	$(3.5 \pm 0.7) \times 10^{16}$	$(0-1.4) \times 10^{15}$	$(5.10 \pm 1.31) \times 10^{-11}$
296 ± 2	2.88×10^{16}	$(0-9.4) \times 10^{14}$	$(1.56 \pm 0.18) \times 10^{-11}$
296 ± 2	4.8×10^{16}	$(0-9.2) \times 10^{14}$	$(1.93 \pm 0.21) \times 10^{-11}$ [b]
296 ± 2	4.8×10^{16}	$(0-9.2) \times 10^{14}$	$(1.79 \pm 0.19) \times 10^{-11}$ [b]
296 ± 2	4.83×10^{16}	$(0-1.6) \times 10^{15}$	$(1.78 \pm 0.19) \times 10^{-11}$
296 ± 2	8.35×10^{16}	$(0-2.7) \times 10^{15}$	$(1.85 \pm 0.19) \times 10^{-11}$
296 ± 2	1.08×10^{17}	$(0-1.9) \times 10^{15}$	$(1.90 \pm 0.21) \times 10^{-11}$
296 ± 2	1.66×10^{17}	$(0-1.5) \times 10^{15}$	$(2.06 \pm 0.23) \times 10^{-11}$
296 ± 2	1.76×10^{17}	$(0-6.9) \times 10^{14}$	$(2.00 \pm 0.21) \times 10^{-11}$ [b]
296 ± 2	2.34×10^{17}	$(0-1.2) \times 10^{15}$	$(2.12 \pm 0.22) \times 10^{-11}$
296 ± 2	3.28×10^{17}	$(0-1.1) \times 10^{15}$	$(2.30 \pm 0.28) \times 10^{-11}$
296 ± 2	4.85×10^{17}	$(0-7.8) \times 10^{14}$	$(2.29 \pm 0.23) \times 10^{-11}$
296 ± 2	7.20×10^{17}	$(0-1.3) \times 10^{15}$	$(2.39 \pm 0.34) \times 10^{-11}$
296 ± 2	1.03×10^{18}	$(0-1.1) \times 10^{15}$	$(2.41 \pm 0.29) \times 10^{-11}$
296 ± 2	1.65×10^{18}	$(0-3.3) \times 10^{15}$	$(2.30 \pm 0.29) \times 10^{-11}$
296 ± 2	3.32×10^{18}	$(0-2.7) \times 10^{15}$	$(2.33 \pm 0.29) \times 10^{-11}$

[a] The indicated uncertainties are represented as $\pm 2\sigma_c$, where σ_c is a "combined standard uncertainty" that accumulates both statistical and systematic errors (see text). [b] Taken from our previous paper.[1]

TABLE 4: Rate Constants for the OH + C_4H_8 Reaction (k_3). Buffer Gas N_2

T, K	total gas density, molecule cm^{-3}	$[C_4H_8]$, molecule cm^{-3}	rate constant,[a] cm^3 molecule^{-1} s^{-1}
96 ± 4	$(1.9 \pm 0.2) \times 10^{16}$	$(0-2.1) \times 10^{14}$	$(1.74 \pm 0.28) \times 10^{-10}$
103 ± 9	2.1×10^{16}	$(0-2.9) \times 10^{14}$	$(1.24 \pm 0.27) \times 10^{-10}$ [b]
110 ± 7	$(2.65 \pm 0.45) \times 10^{16}$	$(0-4.5) \times 10^{14}$	$(1.68 \pm 0.40) \times 10^{-10}$
165 ± 14	$(3.5 \pm 0.7) \times 10^{16}$	$(0-6.8) \times 10^{14}$	$(5.80 \pm 1.51) \times 10^{-11}$
165 ± 14	$(3.5 \pm 0.7) \times 10^{16}$	$(0-1.1) \times 10^{15}$	$(8.13 \pm 2.10) \times 10^{-11}$
296 ± 2	2.88×10^{16}	$(0-7.5) \times 10^{14}$	$(3.03 \pm 0.34) \times 10^{-11}$
296 ± 2	4.90×10^{16}	$(0-4.6) \times 10^{14}$	$(3.18 \pm 0.37) \times 10^{-11}$ [b]
296 ± 2	1.57×10^{17}	$(0-5.7) \times 10^{14}$	$(2.94 \pm 0.37) \times 10^{-11}$
296 ± 2	6.96×10^{17}	$(0-1.6) \times 10^{15}$	$(3.03 \pm 0.34) \times 10^{-11}$
296 ± 2	3.34×10^{18}	$(0-2.5) \times 10^{15}$	$(2.88 \pm 0.46) \times 10^{-11}$

[a] The indicated uncertainties are represented as $\pm 2\sigma_c$, where σ_c is a "combined standard uncertainty" that accumulates both statistical and systematic errors (see text). [b] Taken from our previous paper.[1]

uncertainties of the measured rate constants are reported as $2\sigma_c$, where σ_c's are the "combined standard uncertainties" calculated according to NIST recommendations,[17] as described in a previous paper.[1]

Although it would be desirable, a large variation in the total gas number density in the supersonic flow produced by a Laval nozzle is not possible, due to certain technical difficulties and also to the fact that each nozzle is designed for a particular gas density. Therefore, the low-temperature measurements have been performed at a single total gas number density for each temperature. However, at room temperature, we obtained the kinetic data for reactions R1, R2, and R3 over a relatively wide range of total pressure (more than 2 orders of magnitude). The information about the falloff behavior of the rate constants at room temperature is helpful in estimating the importance of the falloff effects for lower temperatures. The solid points in Figure 3 show the room-temperature rate constants for reactions R1, R2, and R3 measured in this work as a function of total gas density (with nitrogen used as a buffer gas). The rate constants obtained by other groups are also shown. For reaction R1, only the data obtained with buffer gases similar to nitrogen (Ar, N_2, synthetic air) are presented. The only exception is the point at a total gas density of 10^{21} molecules cm^{-3} indicating a recent very-high-pressure measurement by Fulle et al. with M = He.[8]

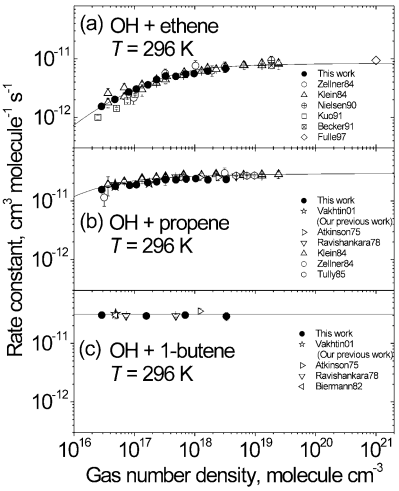

Figure 3. Room-temperature rate constants of reactions R1, R2, and R3 obtained in this work and taken from the literature, plotted as a function of total gas density. Legend: Vakhtin01, Vakhtin et al. (M = N_2);[1] Zellner84, Zellner and Lorenz (M = Ar);[3] Klein84, Klein et al. (M = Ar and synthetic air);[4] Nielsen90, Nielsen et al. (M = Ar);[5] Kuo91, Kuo and Lee (M = N_2);[7] Becker91, Becker et al. (M = synthetic air);[6] Fulle97, Fulle et al. (M = He);[8] Atkinson75, Atkinson and Pitts (M = Ar);[44] Ravishankara78, Ravishankara et al. (M = He);[49] Tully85, Tully and Goldsmith (M = He);[45] Biermann82, Biermann et al. (M = He).[50] Solid lines show the fitted falloff curves (see text).

To obtain the room-temperature falloff parameters, we fitted the experimental data by the Troe expression:[18,19]

$$k = [k_0[\mathrm{M}]/(1 + k_0[\mathrm{M}]/k_\infty)]F \qquad (1)$$

where

$$\log F = \log F_{\mathrm{cent}}/[1 + (\log(k_0[\mathrm{M}]/k_\infty))^2] \qquad (2)$$

In eqs 1 and 2, k_0 and k_∞ are the limiting low-pressure and high-pressure rate constants, respectively; F is the "broadening" correction factor, which takes into account the energy distribution of the back-dissociating adducts and weak collision effects.[18,19] F_{cent} is the value of F at the "center" of the falloff curve (i.e., where $k_0[\mathrm{M}] = k_\infty$). Equation 1 was used to fit our data for reactions R1 and R2 alone and also combined with the literature data shown in Figure 3a,b. For the data obtained in this work, the following parameters were obtained: $k_{1,0} = (11.6 \pm 1.8) \times 10^{-29}$ cm^6 molecule^{-2} s^{-1}, $k_{1,\infty} = (7.5 \pm 0.4) \times 10^{-12}$ cm^3 molecule^{-1} s^{-1}, with $F_{\mathrm{cent}} = 0.65$ for reaction

R1; $k_{2,0} = (9.0 \pm 3.6) \times 10^{-27}$ cm^6 molecule^{-2} s^{-1}, $k_{2,\infty} = (2.6 \pm 0.2) \times 10^{-11}$ cm^3 molecule^{-1} s^{-1}, with $F_{cent} = 0.5$ for reaction R2. When all the data shown in Figure 3a,b were fitted, the following falloff parameters were obtained: $k_{1,0} = (8.6 \pm 1.4) \times 10^{-29}$ cm^6 molecule^{-2} s^{-1}, $k_{1,\infty} = (8.7 \pm 0.4) \times 10^{-12}$ cm^3 molecule^{-1} s^{-1}, with $F_{cent} = 0.65$ for reaction R1; $k_{2,0} = (6.2 \pm 2.0) \times 10^{-27}$ cm^6 molecule^{-2} s^{-1}, $k_{2,\infty} = (3.0 \pm 0.1) \times 10^{-11}$ cm^3 molecule^{-1} s^{-1}, with $F_{cent} = 0.5$ for reaction R2. The broadening factors F_{cent} were estimated as recommended by Troe and co-workers[18,19] (see below). Since the fitted low- and high-pressure rate constants showed good agreement with the latest recommended values,[16,20,21] we adopted the following recommended falloff parameters: $k_{1,0} = 9 \times 10^{-29}$ cm^6 molecule^{-2} s^{-1}, $k_{1,\infty} = 9 \times 10^{-12}$ cm^3 molecule^{-1} s^{-1}, $F_{cent} = 0.65$ for reaction R1;[21] $k_{2,0} = 8 \times 10^{-27}$ cm^6 molecule^{-2} s^{-1}, $k_{2,\infty} = 3.0 \times 10^{-11}$ cm^3 molecule^{-1} s^{-1}, $F_{cent} = 0.5$ for reaction R2.[21] The falloff curves constructed with these parameters are shown in Figure 3a,b.

Reaction R3 does not show any noticeable pressure dependence; thus its rate constant is considered to be in its high-pressure limit under the experimental conditions employed in this work, for both low-temperature and room-temperature measurements. Simple averaging of the data shown in Figure 3c yields the following rate constants: $k_{3,\infty} = (3.0 \pm 0.2) \times 10^{-11}$ cm^3 molecule^{-1} s^{-1} (data from this work only) and $k_{3,\infty} = (3.1 \pm 0.4) \times 10^{-11}$ cm^3 molecule^{-1} s^{-1} (this work and the literature data). The latter value, which is in good agreement with the recommendation by Atkinson,[20] was adopted as $k_{3,\infty}$ and is shown as the solid line in Figure 3c.

For reaction R1, the strong-collision low-pressure rate constants k_0^{SC} were calculated by using the Troe formulas for barrierless association reactions,[22,23] and the collision efficiencies, β_c, were obtained as $\beta_c = k_0/k_0^{SC}$. To calculate k_0^{SC}, we used the vibrational frequencies and structural parameters of the C_2H_4OH adducts reported by Villa et al.[24] and the OH + $C_2H_4 \rightarrow C_2H_4OH$ reaction enthalpy $\Delta H_0^\circ = -123$ kJ/mol that was recently measured by Fulle et al.[8] This experimental value agrees well with the earlier experimental data[25] and ab initio calculations.[9,24,26,27] For reaction R2, the k_0^{SC} values were also estimated. In view of the lack of spectroscopic and thermodynamic information on the C_3H_6OH adduct, only approximate estimates of k_0^{SC} could be made. To get estimates of the vibrational frequencies, the structure of C_3H_6OH, and the enthalpy of reaction R2, we performed Gaussian-98[28] quantum chemical calculations for C_3H_6OH and also C_2H_4OH for comparison, using the CBS-QB3 compound method developed by Montgomery et al.[29,30] For C_2H_4OH, our calculations resulted in vibrational frequencies and structures similar to those reported by Villa et al.[24] The reaction enthalpy was calculated as -113 kJ/mol at 0 K, showing a reasonable agreement with the experimental value. As expected, the CBS-QB3 calculations for reaction R2 gave essentially the same reaction enthalpy as for reaction R1, which encouraged us to use the experimental ΔH_0°, obtained for the OH + $C_2H_4 \rightarrow C_2H_4OH$ reaction,[8] for calculations of k_0^{SC} for reaction R2. It was found that, for reaction R2, the falloff effects, although important at room temperature, are essentially negligible under the low-temperature conditions of the Laval nozzle supersonic expansions employed in our experiments. That is, the rate constants obtained at $T = 96-165$ K and at total gas densities of $(1.9-3.5) \times 10^{16}$ molecule cm^{-3} (see Tables 2−4) are at or very close to the high-pressure limit.

For reaction R1 the situation is more complicated. The falloff effects are important even at low temperatures and need to be taken into account to obtain the high-pressure limiting rate constants at these temperatures. Note, however, that at low temperatures (96−165 K) and gas number densities of $(1.9-3.5) \times 10^{16}$ molecule cm^{-3}, k_1 is close to its high-pressure limit, and the extrapolation of the experimental data to infinite pressure is not very sensitive to the uncertainties of the falloff model. Figure 4 shows the results of fitting each experimental low-temperature data point for reaction R1 by eq 1. During fitting, the calculated low-pressure rate constant k_0 and the falloff central broadening factor F_{cent} were fixed at the values described below, and k_∞ was allowed to float. In calculations of k_0 at low temperatures, we assumed that the average energy transferred per collision $-\langle\Delta E\rangle$ does not depend on temperature. Based on the room-temperature β_c value, the $-\langle\Delta E\rangle$ value was estimated to be equal to 115 cm^{-1}, using the following expression: $\beta_c/(1 - \beta_c^{1/2}) = -\langle\Delta E\rangle/(F_E kT)$, where F_E is the correction factor for the energy dependence of the vibrational density of states at the adduct dissociation threshold.[22,31] Then the β_c values for lower temperatures were calculated for $-\langle\Delta E\rangle = 115$ cm^{-1}. The central broadening factor F_{cent} was represented as a product of "strong-collision" and "weak-collision" factors: $F_{cent} = F_{cent}^{SC} F_{cent}^{WC}$.[18,19] The F_{cent}^{SC} factor was estimated as recommended by Troe,[18] with the vibrational frequencies of the transition state taken from ab initio calculations by Villa et al.[24] The weak-collision broadening factor F_{cent}^{WC} was obtained by using the expression $\log F_{cent}^{WC} = 0.14 \log \beta_c$.[19] The falloff parameters for reaction R1 are shown in Table 5.

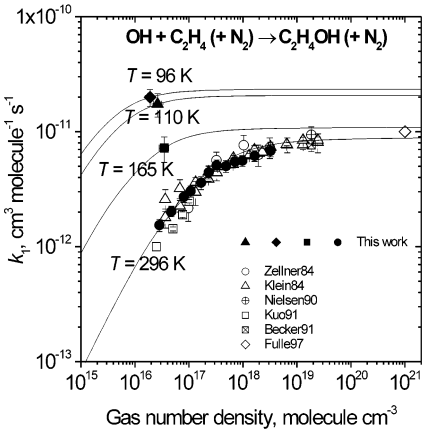

Figure 4. Solid points: experimental rate constants for reaction (R1) measured in this work at temperatures of 296, 165, 110, and 96 K plotted as a function of total gas density. Open points: room-temperature data obtained by other groups: Zellner84: Zellner and Lorenz (M = Ar);[3] Klein84: Klein et al. (M = Ar and synthetic air);[4] Nielsen90: Nielsen et al. (M = Ar);[5] Kuo91: Kuo and Lee (M = N_2);[7] Becker91: Becker et al. (M = synthetic air);[6] Fulle97: Fulle et al. (M = He).[8] For $T = 296$ K, the line shows the fit of all the experimental data by the Troe expression.[18,19] The lines for $T = 165$, 110, and 96 K are the extrapolations of the experimental data obtained at a single total gas density to the high-pressure limit, using calculated low-pressure limiting rate constants (see text).

The resulting high-pressure rate constants for reactions R1−R3 are plotted as a function of temperature in Figure 5. The error bars for $k_{1,\infty}$ include the systematic error, in addition to the statistical error. The systematic error arises from the uncertainty of the extrapolation of the kinetic data to the high-pressure limit, which is dominated by the uncertainty in the calculated $k_{1,0}$ values. Under a rather conservative assumption that the calculated $k_{1,0}$ values are accurate to a factor of 2, we estimated the systematic error as the range of the $k_{1,\infty}$ variation when the low-pressure rate constant was varied from $0.5k_{1,0}$ to $2k_{1,0}$. Then the combined uncertainty that includes the systematic

TABLE 5: Falloff Parameters for the OH + C_2H_4 (+ N_2) → C_2H_4OH (+ N_2) Reaction

T, K	k_0^{SC},[a] cm^6 molecule^{-2} s^{-1}	β_c	F_{cent}^{SC}	F_{cent}^{WC}	F_{cent}	k_0, cm^6 molecule^{-2} s^{-1}	k_∞, cm^3 molecule^{-1} s^{-1}
296	3.7×10^{-28}	0.24	0.79	0.82	0.65	9.0×10^{-29}	9.0×10^{-12}
165	2.9×10^{-27}	0.36	0.93	0.87	0.81	1.0×10^{-27}	1.1×10^{-11}
110	1.2×10^{-26}	0.46	1.0	0.90	0.90	5.7×10^{-27}	2.1×10^{-11}
96	2.0×10^{-26}	0.49	1.0	0.90	0.90	9.8×10^{-27}	2.4×10^{-11}

[a] Calculated by the Troe method.[22,23]

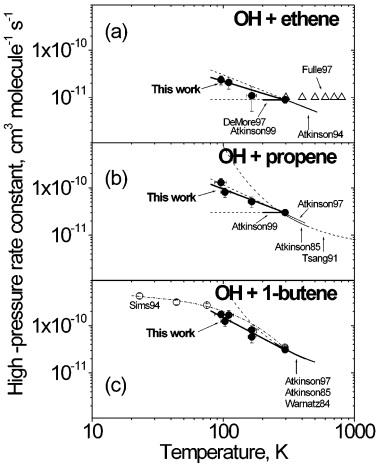

Figure 5. High-pressure rate constants of reactions R1, R2, and R3 plotted as a function of temperature. Filled points are the results of the present measurements. Open triangles in (a) are the experimental high-pressure rate constants reported by Fulle et al.[8] Open circles and dash−dot line in (c) are the low-temperature data for reaction R3 obtained in the CRESU apparatus.[15] Thick solid lines show the fits of the data obtained in this work by the empirical expression $k = A(T/300)^n$ (see eqs 3−5). Thin lines represent the recommended high-temperature rate constants: Warnatz84, Warnatz;[32] Atkinson85, Atkinson;[33] Tsang91, Tsang;[34] Atkinson97, Atkinson;[20] DeMore97, DeMore et al.;[16] Atkinson99, Atkinson et al.[21] Dashed lines show the extrapolations of the recommended high-temperature rate constants to low temperatures.

and statistical contributions was calculated.[17] The three rate constants each show an apparent negative temperature dependence. For reactions R2 and R3, the rate constants measured in this work agree well with our earlier results[1] and the CRESU low-temperature data set (for reaction R3).[15] Thick solid lines in Figure 5 represent the results of the $1/\sigma^2$-weighted fitting of the present data together with the data from the previous work[1] by the empirical expression $k = A(T/300)^n$ used in the IUPAC[21] and NASA[16] evaluations, with two fitting parameters A and n. The temperature dependence of the high-pressure rate constants of reactions R1−R3 can be expressed as follows (for $T = 96-296$ K):

$$k_{1,\infty} = (8.7 \pm 0.7) \times 10^{-12}(T/300)^{(-0.85\pm0.11)} \text{ cm}^3 \text{ molecule}^{-1} \text{ s}^{-1} \quad (3)$$

$$k_{2,\infty} = (2.95 \pm 0.10) \times 10^{-11}(T/300)^{(-1.06\pm0.13)} \text{ cm}^3 \text{ molecule}^{-1} \text{ s}^{-1} \quad (4)$$

$$k_{3,\infty} = (3.02 \pm 0.15) \times 10^{-11}(T/300)^{(-1.44\pm0.10)} \text{ cm}^3 \text{ molecule}^{-1} \text{ s}^{-1} \quad (5)$$

The literature data for reactions R1−R3, represented by the evaluated rate constants from the reviews,[16,20,21,32−35] are also presented in Figure 5. For reaction R1, DeMore et al. (NASA evaluation)[16] and Atkinson et al. (IUPAC evaluation)[21] recommend temperature-independent values of 8.8×10^{-12} and 9×10^{-12} cm^3 molecule^{-1} s-^{1}, respectively, for the temperature range of $T = 200-300$ K. For higher temperatures ($T = 290-525$ K), the rate constant $k_{1,\infty} = 9 \times 10^{-12}(T/298)^{-1.1}$ cm^3 molecule^{-1} s^{-1} with a slight negative temperature dependence is recommended by Atkinson.[20,35] The latter expression extrapolated down to $T = 90$ K describes the experimental low-temperature data reasonably well, overestimating $k_{1,\infty}$ by a factor of ≈1.5 at $T = 100$ K. The IUPAC[21] and NASA[16] evaluations significantly underestimate $k_{1,\infty}$ at low temperatures.

For reaction R2, IUPAC evaluation[21] recommends a temperature-independent value of 3.0×10^{-11} cm^3 molecule^{-1} s^{-1} ($T = 200-300$ K), while for higher temperatures ($T = 290-525$ K) the following rate constant is suggested by Atkinson:[20] $k_{2,\infty} = 2.8 \times 10^{-11}(T/298)^{-1.3}$ cm^3 molecule^{-1} s^{-1}. Again, the extrapolated higher temperature expression[20] is the most appropriate. The IUPAC evaluation[21] underestimates $k_{2,\infty}$ at low temperatures, while the earlier evaluations by Atkinson[33] and Tsang,[34] when extrapolated down to $T = 90$ K, yield very high rate constants that are not physically reasonable.

For reaction R3, the available reviews by Warnatz[32] and Atkinson[33] recommend the Arrhenius expression with a negative activation energy of about −3.8 kJ/mol (−0.9 kcal/mol), which is obviously inadequate for extrapolation to low temperature.

The negative temperature dependence of the rate constants for reactions of OH radical with alkenes has been a matter of extensive discussions.[24,33,36−38] Some of the explanations involve an assumption of the formation of an intermediate weakly bound complex[36,38] followed by competing forward and backward dissociation of the complex.[39−41] Villa et al.[24] applied variational transition state theory on the calculated potential energy surface for the OH + C_2H_4 reaction and managed to reproduce the experimental negative temperature dependence of k_1 without any assumptions about the intermediate complex formation. It could be also possible that, at low temperatures, the reaction rate is controlled by adiabatic capture on the attractive part of the barrierless potential energy surface that is determined by long-range electrostatic interactions.[37] As the temperature is lowered, the inter-reagent distance, corresponding to the transition state, increases, until eventually the reaction rate is determined by the capture.[37] For reaction of a $^2\Pi$ dipole with a $^1\Sigma$ quadrupole, for moderately low temperatures, adiabatic capture theory predicts rate constants independent of temperature.[37,42,43] The experimental $k_{1,\infty}$, $k_{2,\infty}$, and $k_{3,\infty}$ each show a trend of increasing value with decreasing temperature; however, there are signs of leveling-off at the lowest temperatures,[15] which could indicate approaching the capture limit.[37]

Fulle et al.[8] performed measurements of k_1 at very high pressures (total gas densities of He up to 10^{21} molecule cm^{-3}). They succeeded in approaching high-pressure conditions for this reaction for temperatures as high as 800 K. Their data show essentially no temperature dependence of $k_{1,\infty}$ for $T = 300-800$ K. These results disagree with many earlier measurements that show a negative temperature dependence for $k_{1,\infty}$. In view of the experiments by Fulle et al.,[8] it could be argued that the apparent negative temperature dependence of $k_{1,\infty}$ is the result of improper extrapolation of the data, obtained in the intermediate pressure range, to the high-pressure limit. However, this

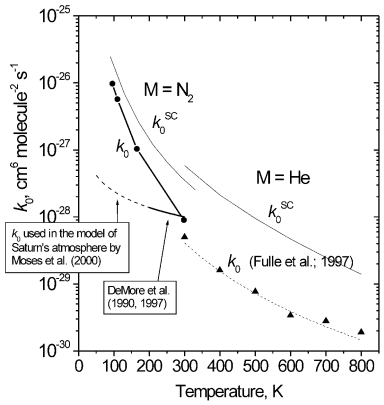

Figure 6. Low-pressure limiting rate constant for reaction R1. Filled circles show $k_{1,0}$ calculated in this work. Filled triangles and dashed line are the experimental $k_{1,0}$ obtained by Fulle et al.[8] Solid lines, marked as k_0^{SC}, are the strong-collision rate constants calculated in this work by the Troe method[22,23] for M = N_2 and M = He. Also shown are the temperature dependence of $k_{1,0}$, recommended for $T = 200-300$ K by DeMore et al.[16] (solid line) and its extrapolation to low temperatures (dashed line) that is used in the photochemical model of Saturn's atmosphere by Moses et al.[46]

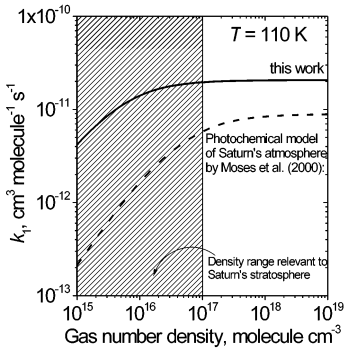

Figure 7. Pressure dependence of k_1 calculated for $T = 110$ K with the falloff parameters obtained in this work for M = N_2 (solid line) and with those used in the photochemical model of Saturn's atmosphere by Moses et al.[46] (dashed line). The shaded area represents the gas density range that is relevant to Saturn's stratosphere.

argument can hardly be applied to reactions R2 and R3, which should be at or close to the high-pressure limit at room temperature and moderately elevated temperatures, within the range of total pressures typically used in experimental kinetic studies. The available experimental data on reactions R2 and R3 support a negative temperature dependence of $k_{2,\infty}$ and $k_{3,\infty}$.[3,44,45] It seems that it would be valuable to have further theoretical and experimental studies of the kinetics of the reactions of OH radical with alkenes that may involve measurements under extreme conditions including very low temperatures and very high pressures.

Applications to Photochemical Modeling of Saturn's Atmosphere. In Saturn's atmosphere, reactions of the OH radical with unsaturated hydrocarbons play the key role in conversion of water, introduced mostly by comets and meteors, to molecules containing C−O bonds, ultimately CO and CO_2.[46] According to the model by Moses et al.,[46] the two most important reactions following dissociation of H_2O by photolysis are OH + C_2H_2 and OH + C_2H_4. In view of the lack of experimental data, the most straightforward way to obtain estimates for low-temperature rate constants is extrapolation of the literature high-temperature rate constants to the temperature and pressure range that are important for Saturn's stratosphere. In many cases, however, these extrapolations lead to significant errors.[47] To estimate the low-temperature rate constants of the OH + C_2H_4 reaction, Moses et al.[46] extrapolated the expressions for $k_{1,\infty}$ and $k_{1,0}$ evaluated by DeMore et al.[48] Thus, $k_{1,\infty}$ was considered temperature-independent and equal to $k_{1,\infty} = 8.79 \times 10^{-12}$ cm^3 molecule^{-1} s^{-1}.[48] For the low-pressure rate constant, the following expression was adopted: 9.59×10^{-27} $T^{-0.8}$ cm^6 molecule^{-2} s^{-1}.[48] This expression, extrapolated to low temperatures, is shown as a dashed line in Figure 6. It is seen from Figure 6 that the extrapolated low-pressure rate constant does not agree well with the value of $k_{1,0}$ estimated in this work (based on the room-temperature falloff analysis) and the experimental values obtained by Fulle et al.[8]

Figure 7 compares the falloff curve for reaction R1 at $T = 110$ K obtained in this work for M = N_2 (solid curve) and the falloff curve constructed with the extrapolated kinetic parameters used by Moses et al.[46] (dashed curve). It follows from Figure 7 that, for the pressure range essential for Saturn's stratosphere, the difference is significant (about an order of magnitude). Since the most abundant gas in the Saturn's atmosphere is hydrogen, it would be more appropriate to use $k_{1,0}$ for M = H_2 to construct the falloff curve. Our estimates show that $k_{1,0}$ for M = H_2 will be about 60% larger than $k_{1,0}$ for M = N_2, thus making the difference between the falloff curve based on the experimental data and that used in the photochemical model[46] even more dramatic.

Although it is difficult to predict the detailed impact of the new low-temperature experimental rate constant for reaction R1 on the Saturn atmospheric models, rough estimates can be made. According to the photochemical model by Moses et al.,[46] in Saturn's stratosphere, about 96% of the water that is photodissociated into H and OH efficiently recycles (mostly through the OH + H_2 reaction). The remaining 4% of photochemical loss of water results in permanent conversion of H_2O into CO and CO_2 (70%) and condensation (30%). The most important primary processes that are responsible for the conversion of water to carbon oxides are the OH + C_2H_2 and OH + C_2H_4 reactions. In the calculated reaction rate profiles,[46] the rate of OH + C_2H_2 is about an order of magnitude higher than that of the OH + C_2H_4 reaction. However, if the experimental low-temperature rate constant for the OH + C_2H_4 reaction were used, the two reaction rates would be approximately the same. This would probably lead to about a 2-fold increase in the overall rate of permanent photochemical conversion of H_2O to CO and CO_2 and would therefore affect the calculated balance of conversion/condensation of water. This example shows the importance of direct kinetic measurements at low temperatures for adequate photochemical modeling of planetary atmospheres.

Acknowledgment. The support of this research by the National Aeronautics and Space Administration (Grants NAG5-8923 and NAG5-13339) is gratefully acknowledged.

References and Notes

(1) Vakhtin, A. B.; Lee, S.; Heard, D. E.; Smith, I. W. M.; Leone, S. R. *J. Phys. Chem. A* **2001**, *105*, 7889.
(2) Tully, F. P. *Chem. Phys. Lett.* **1983**, *96*, 198.
(3) Zellner, R.; Lorenz, K. *J. Phys. Chem.* **1984**, *88*, 984.
(4) Klein, T.; Barnes, I.; Becker, K. H.; Fink, E. H.; Zabel, F. *J. Phys. Chem.* **1984**, *88*, 5020.
(5) Nielsen, O. J.; Jorgensen, O.; Donlon, M.; Sidebottom, H. W.; O'Farrell, D. J.; Treacy, J. *Chem. Phys. Lett.* **1990**, *168*, 319.
(6) Becker, K. H.; Geiger, H.; Wiesen, P. *Chem. Phys. Lett.* **1991**, *184*, 256.
(7) Kuo, C. H.; Lee, Y. P. *J. Chem. Phys.* **1991**, *95*, 1253.
(8) Fulle, D.; Hamann, H. F.; Hippler, H.; Jansch, C. P. *Ber. Bunsen-Ges. Phys. Chem.* **1997**, *101*, 1433.
(9) Hippler, H.; Viskolcz, B. *Phys. Chem. Chem. Phys.* **2000**, *2*, 3591.

(10) Lee, S.; Hoobler, R. J.; Leone, S. R. *Rev. Sci. Instrum.* **2000**, *71*, 1816.
(11) Liepmann, H. W.; Roshko, A. *Elements of Gasdynamics*; Wiley: New York, 1957.
(12) Kijewski, H.; Troe, J. *Helv. Chim. Acta* **1972**, *55*, 205.
(13) Nicovich, J. M.; Wine, P. H. *J. Geophys. Res.* **1988**, *93*, 2417.
(14) Kliner, D. A. V.; Farrow, R. L. *J. Chem. Phys.* **1999**, *110*, 412.
(15) Sims, I. R.; Smith, I. W. M.; Bocherel, P.; Defrance, A.; Travers, D.; Rowe, B. R. *J. Chem. Soc., Faraday Trans.* **1994**, *90*, 1473.
(16) DeMore, W. B.; Sander, S. P.; Golden, D. M.; Hampson, R. F.; Kurylo, M. J.; Howard, C. J.; Ravishankara, A. R.; Kolb, C. E.; Molina, M. J. *JPL Publication 97-4*, 1997.
(17) Taylor, B. N.; Kuyatt, C. E. *Guidelines for Evaluating and Expressing the Uncertainty of NIST Measurement Results, NIST Technical Note 1297*; US Government Printing Office: Washington, DC, 1994.
(18) Troe, J. *Ber. Bunsen-Ges. Phys. Chem. Chem. Phys.* **1983**, *87*, 161.
(19) Gilbert, R. G.; Luther, K.; Troe, J. *Ber. Bunsen-Ges. Phys. Chem. Chem. Phys.* **1983**, *87*, 169.
(20) Atkinson, R. *J. Phys. Chem. Ref. Data* **1997**, *26*, 215.
(21) Atkinson, R.; Baulch, D. L.; Cox, R. A.; Hampson, R. F.; Kerr, J. A.; Rossi, M. J.; Troe, J. *J. Phys. Chem. Ref. Data* **1999**, *28*, 191.
(22) Troe, J. *J. Chem. Phys.* **1977**, *66*, 4745.
(23) Troe, J. *J. Chem. Phys.* **1977**, *66*, 4758.
(24) Villa, J.; Gonzalez-Lafont, A.; Lluch, J. M.; Corchado, J. C.; Espinosa-Garcia, J. *J. Chem. Phys.* **1997**, *107*, 7266.
(25) Diau, E. W. G.; Lee, Y. P. *J. Chem. Phys.* **1992**, *96*, 377.
(26) Sosa, C.; Schlegel, H. B. *J. Am. Chem. Soc.* **1987**, *109*, 7007.
(27) Piqueras, M. C.; Crespo, R.; Nebot-Gil, I.; Tomas, F. *Theochem.-J. Mol. Struct.* **2001**, *537*, 199.
(28) Frisch, M. J.; Trucks, G. W.; Schlegel, H. B.; Scuseria, G. E.; Robb, M. A.; Cheeseman, J. R.; Zakrzewski, V. G.; Montgomery, J. A., Jr.; Stratmann, R. E.; Burant, J. C.; Dapprich, S.; Millam, J. M.; Daniels, A. D.; Kudin, K. N.; Strain, M. C.; Farkas, O.; Tomasi, J.; Barone, V.; Cossi, M.; Cammi, R.; Mennucci, B.; Pomelli, C.; Adamo, C.; Clifford, S.; Ochterski, J.; Petersson, G. A.; Ayala, P. Y.; Cui, Q.; Morokuma, K.; Malick, D. K.; Rabuck, A. D.; Raghavachari, K.; Foresman, J. B.; Cioslowski, J.; Ortiz, J. V.; Baboul, A. G.; Stefanov, B. B.; Liu, G.; Liashenko, A.; Piskorz, P.; Komaromi, I.; Gomperts, R.; Martin, R. L.; Fox, D. J.; Keith, T.; Al-Laham, M. A.; Peng, C. Y.; Nanayakkara, A.; Gonzalez, C.; Challacombe, M.; Gill, P. M. W.; Johnson, B. G.; Chen, W.; Wong, M. W.; Andres, J. L.; Head-Gordon, M.; Replogle, E. S.; Pople, J. A. Gaussian 98; 5.1 ed.; Gaussian, Inc.,: Pittsburgh, PA, 1998.
(29) Montgomery, J. A.; Frisch, M. J.; Ochterski, J. W.; Petersson, G. A. *J. Chem. Phys.* **1999**, *110*, 2822.
(30) Montgomery, J. A.; Frisch, M. J.; Ochterski, J. W.; Petersson, G. A. *J. Chem. Phys.* **2000**, *112*, 6532.
(31) Troe, J. *J. Phys. Chem.* **1979**, *83*, 118.
(32) Warnatz, J. Rate Coefficients in the C/H/O system. In *Combustion Chemistry*; Gardiner, W. C., Jr., Ed.; Springer-Verlag: New York, 1984.
(33) Atkinson, R. *Chem. Rev.* **1985**, *85*, 69.
(34) Tsang, W. *J. Phys. Chem. Ref. Data* **1991**, *20*, 221.
(35) Atkinson, R. *J. Phys. Chem. Ref. Data* **1994**, *Monograph 2*, 1.
(36) Singleton, D. L.; Cvetanovic, R. J. *J. Am. Chem. Soc.* **1976**, *98*, 6812.
(37) Smith, I. W. M. *Int. J. Mass Spectrom. Ion Process.* **1995**, *150*, 231.
(38) Alvarez-Idaboy, J. R.; Mora-Diez, N.; Vivier-Bunge, A. *J. Am. Chem. Soc.* **2000**, *122*, 3715.
(39) Mozurkewich, M.; Benson, S. W. *J. Phys. Chem.* **1984**, *88*, 6429.
(40) Chen, Y.; Rauk, A.; Tschuikow-Roux, E. *J. Phys. Chem.* **1991**, *95*, 9900.
(41) Troe, J. *J. Chem. Soc., Faraday Trans.* **1994**, *90*, 2303.
(42) Clary, D. C. *Annu. Rev. Phys. Chem.* **1990**, *41*, 61.
(43) Clary, D. C.; Stoecklin, T. S.; Wickham, A. G. *J. Chem. Soc., Faraday Trans.* **1993**, *89*, 2185.
(44) Atkinson, R.; Pitts, J. N., Jr. *J. Chem. Phys.* **1975**, *63*, 3591.
(45) Tully, F. P.; Goldsmith, J. E. M. *Chem. Phys. Lett.* **1985**, *116*, 345.
(46) Moses, J. I.; Lellouch, E.; Bezard, B.; Gladstone, G. R.; Feuchtgruber, H.; Allen, M. *Icarus* **2000**, *145*, 166.
(47) Sims, I. R.; Smith, I. W. M. *Annu. Rev. Phys. Chem.* **1995**, *46*, 109.
(48) DeMore, W. B.; Golden, D. M.; Hampson, R. F.; Howard, C. J.; Kurylo, M. J.; Molina, L. T.; Ravishankara, A. R.; Sander, S. P. *JPL Publication 90-1* **1990**.
(49) Ravishankara, A. R.; Wagner, S.; Fischer, S.; Smith, G.; Schiff, R.; Watson, R. T.; Tesi, G.; Davis, D. D. *Int. J. Chem. Kinet.* **1978**, *10*, 783.
(50) Biermann, H. W.; Harris, G. W.; Pitts, J. N., Jr. *J. Phys. Chem.* **1982**, *86*, 2958.